FATIGUE AND TENSILE FRACTURE SURFACE MORPHOLOGIES OF ADDITIVE MANUFACTURED AUSTENITIC STAINLESS STEEL

Penn RAWN, Vadiraja SUDHAKAR*

Montana Technological University, Butte, MT 59701, USA

Abstract

Fatigue and tensile fracture surface morphologies of laser additive manufactured (LAM) stainless steel (using powder bed fusion method) were investigated. Both fatigue and tensile fracture surface morphologies were determined using LEO-VP SEM instrument. The fracture surface features were studied as a function of global energy density, one of the main LPBF processing parameters used in producing 316L SS test specimens. The fracture surface morphologies were also compared with the wrought 316L SS fractured specimens. It has been demonstrated that relatively higher energy density (irrespective of the specimen build angle orientations) specimens resulted in predominantly ductile fracture, while lower energy produced relatively brittle fracture surface characteristics, in tensile fractured specimens. Among fatigue fractured specimens, LPBF processed specimens at 90° build angle demonstrated relatively higher ductile fracture characteristics.

Keywords: *fracture morphologies, 316L stainless steel, laser powder bed fusion processing (LPBF), fatigue and tensile fractures.*

Introduction

Laser additive manufacturing (LAM) involves producing desired products layer by layer, based on a 3D model generated from a computer modeling [1, 2]. Additive manufacturing replaces conventional processing methods to produce complex parts in a repetitive manner. LAM is used for producing varieties of engineering metal alloy components. A powder bed is created by raking powder across the work area. Microstructural results have been reported [3] based on the fatigue test of stainless steel material wherein grain boundaries were reported to be the sites for crack initiation leading to final fracture. Austenitic phase in stainless steels is soft and ductile in comparison to brittle martensitic structure. As a result, it has high ductility that reduces notch sensitivity. Solidification structures resulting from additive manufacturing are therefore extensively studied to determine their influence on the final fracture properties. Excessive hardening of the grain boundaries as a result of diffusion of molybdenum [4] element in austenitic stainless steels was the cause for premature fracture and low strength. Zhang et al. [5] work highlights the relationship between structure and property on end properties of the stainless steel components. There are quite a few recent research investigations [6-16] that focused on physical, mechanical, microstructure, fracture properties of stainless steel produced by additive manufacturing.

Processing-microstructure-property-fracture interrelationships are useful to enhance product performance in a given application. In this regard, the information on static and dynamic fracture morphologies are very useful in optimizing processing parameters (specimen build angle orientations and global energy density) to target the expected level of mechanical performance. The aim of this investigation is to determine the fracture mode/s and relate them to LPBF process parameters for 316L stainless steel.

Corresponding author: kvsudhakar@mtech.edu

Experimental Procedure

Metal Alloy Used

Austenitic stainless steel was the metal alloy investigated that consisted of the major alloying elements; C: 0.02, Cr: 16.9, Ni: 12.1, Mo: 2.4, balance iron, all in weight percent.

Tensile and Fatigue Testing

ASTM-E8 standard was used as a reference for performing standard tensile tests. Basic tensile properties were evaluated using MTS Landmark servo hydraulic testing machine. The sample had a cross-section with a diameter of 8.96 mm with 35.6 mm gage length. Fatigue test was performed based on the tensile strength value obtained from the tensile test. Fatigue tests were conducted as per the ASTM standards E2948 and E1823 using continuous radius specimens. The fractured specimens were utilized for the fracture surface investigations.

Results and Discussion

Fatigue fracture surface investigations were performed at crack initiation, propagation, and final fracture zones of the fractured specimens.

Fatigue Fractured Specimens

Wrought Specimens

Figure 1a and 1b show the locations of crack initiation with the evidence of crack and folded material, respectively. The characteristic striation marks are evident in Figure 1c. The classical features of ductile fracture (voids, ductile ridges, dimples) are visible in Figure 1d.
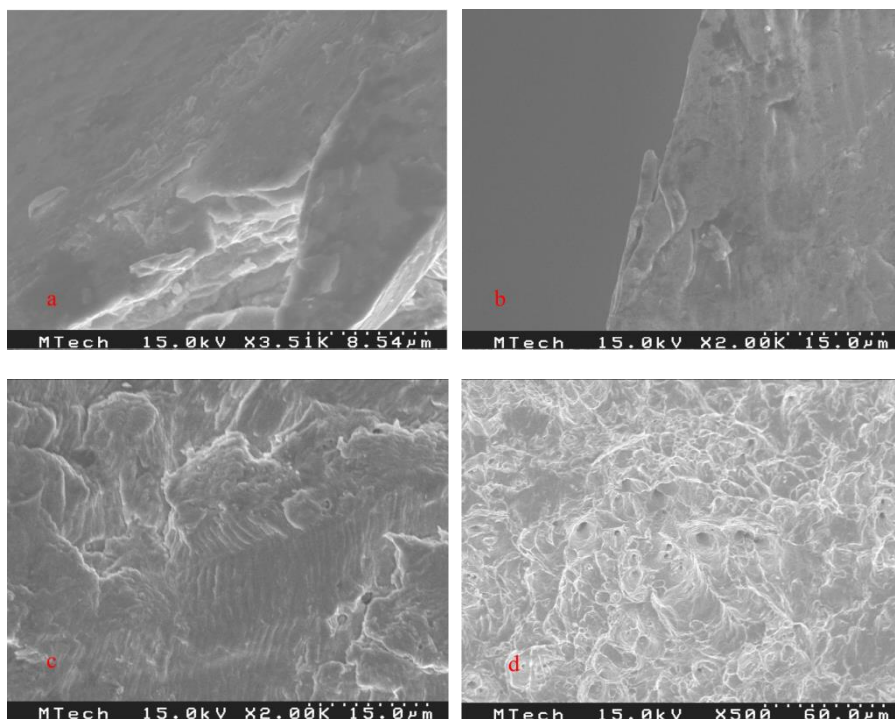

Fig. 1. Fatigue fracture surface features of wrought specimens:
(a, b) for crack initiation, and (c), (d) for crack propagation and final fracture zones, respectively

Specimens with 0° orientation

Figure 2 demonstrates the fatigue fracture surface features of specimens with 0° orientation. Crack initiation is shown in Figure 2a, and Figure 2b shows the same feature at a higher magnification revealing pores. Figure 2c and 2d show characteristic fatigue striations and faceted voids, respectively.
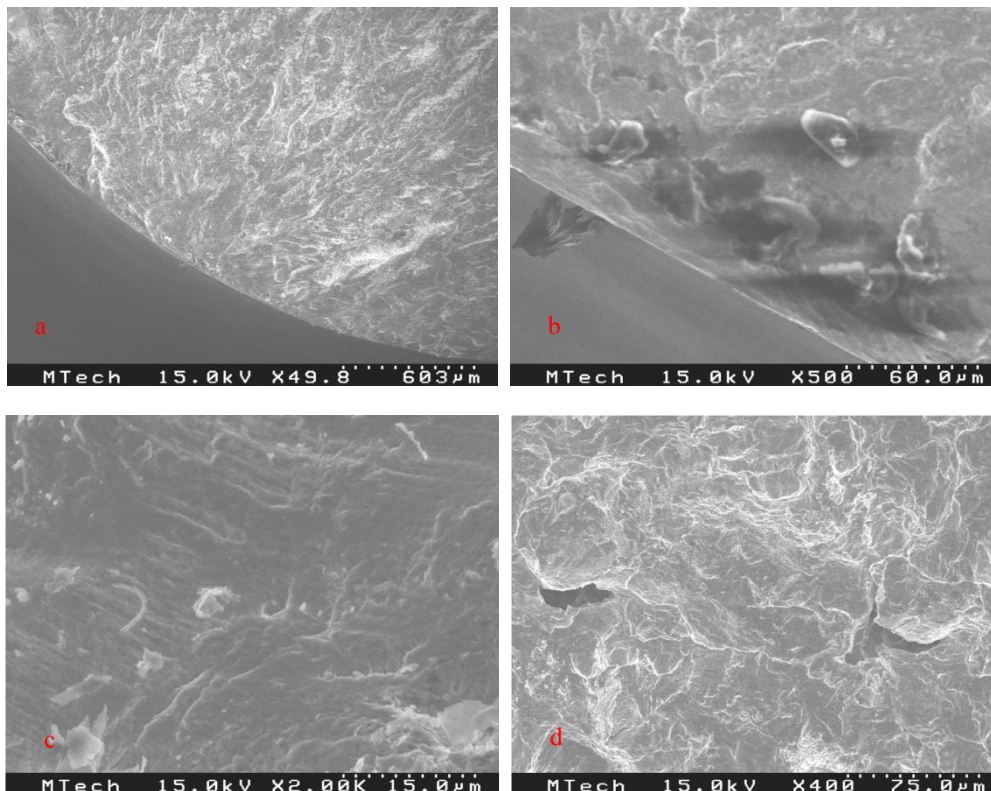

Fig. 2. Fatigue fracture surface features of 0° orientation specimens:
(a, b) for crack initiation, and (c), (d) for crack propagation and final fracture zones, respectively

Specimens with 30° orientation

Crack initiation process is revealed in Figure 3a, as well as in Figure 3b, showing the presence of unmelted particles. The characteristic striation marks are visible in Figure 3c. Figure 3d depicts the region of final fracture with secondary cracks.

Specimens with 60° orientation

Figure 4a and 4b demonstrate crack initiation zone with voids. As demonstrated in the previous cases, striations are visible in Figure 4c and the final fracture surface features in Figure 4d.

Specimens with 90° orientation

Figure 5a and 5b show voids that are responsible for the crack initiation process. Final fracture zone surface features are demonstrated in Figure 5c and 5d showing mostly ductile fracture features.
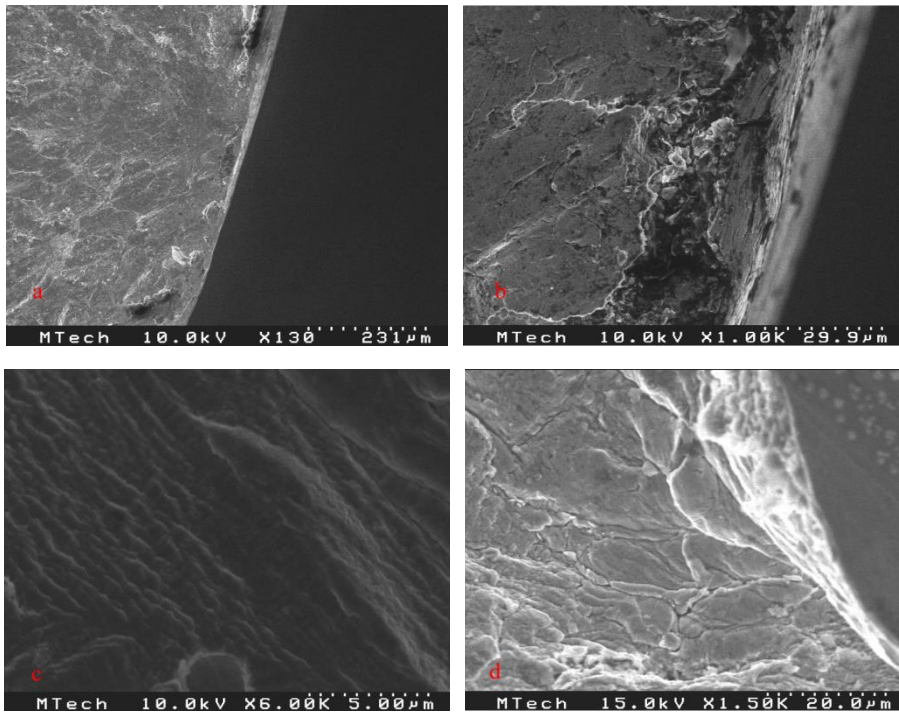
Fig. 3. Fatigue fracture surface features of 30° orientation specimens:
(a, b) for crack initiation, and (c), (d) for crack propagation and final fracture zones, respectively
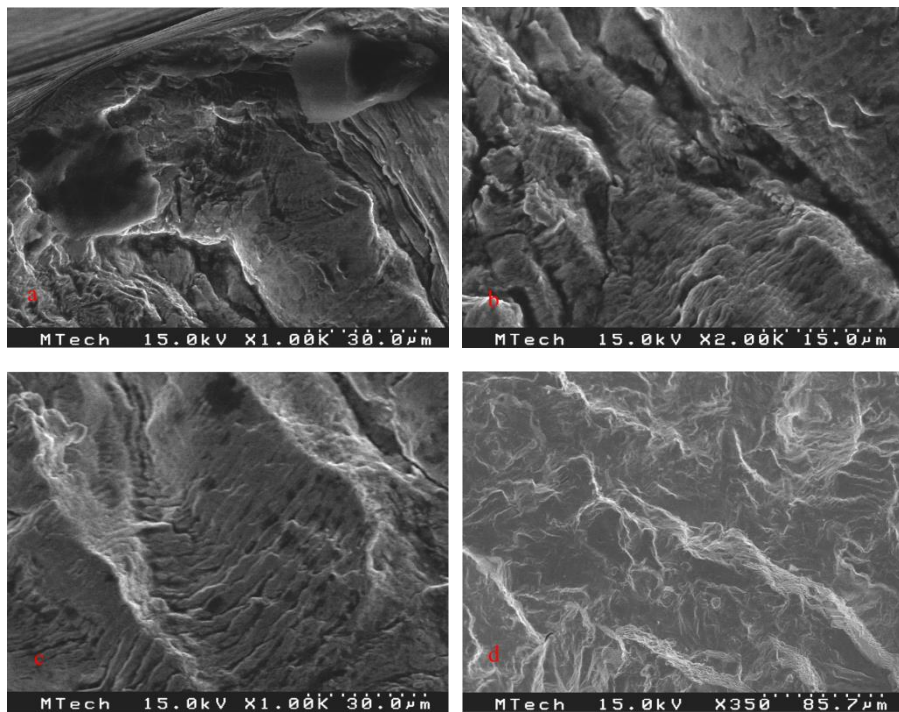

Fig. 4. Fatigue fracture surface features of 60° orientation specimens:
(a, b) for crack initiation, and (c), (d) for crack propagation and final fracture zones, respectively
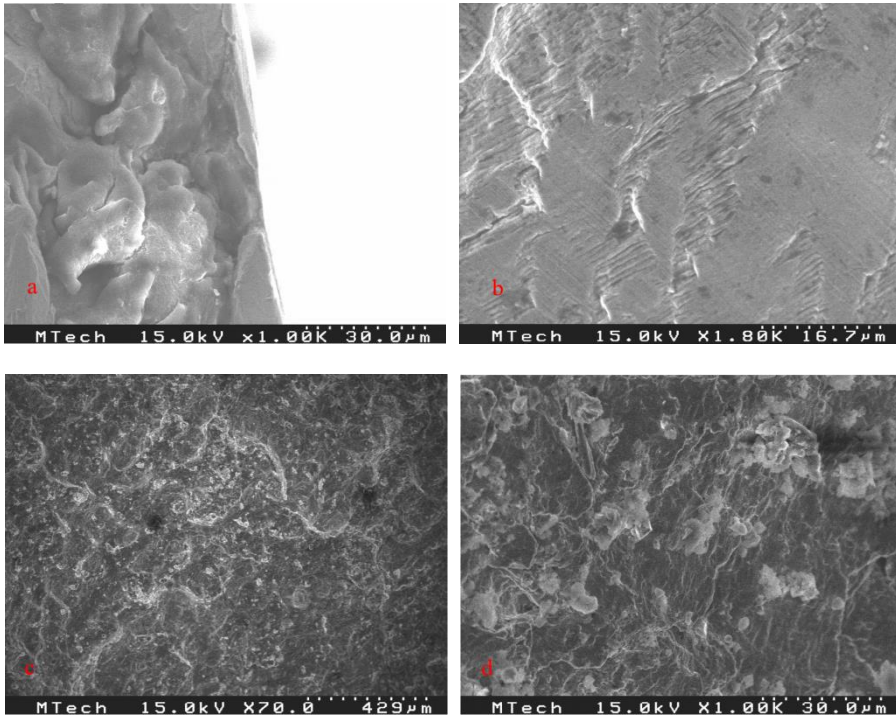
Fig. 5. Fatigue fracture surface features of 90° orientation specimens:
(a, b) for crack initiation, and (c), (d) for final fracture zones, respectively

Tensile fractured specimens

Tensile fracture morphology of 1.67 J/mm² energy density specimen.

Global energy density (*GED*) was calculated using the relation, GED = *P/vh*, where P=laser power (W), v=travel speed (mm/s), and h=hatch spacing (mm).
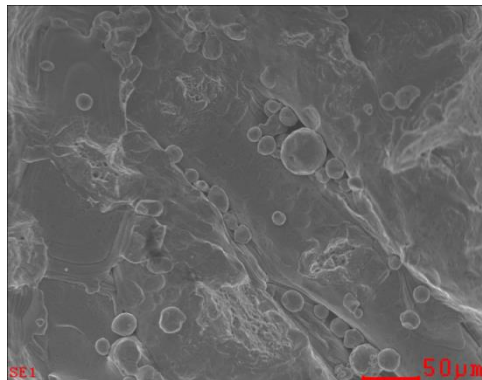

Fig. 6. Tensile fracture (energy density, 1.67 J/mm²) surface showing unmelted particles and partial fusion

Tensile fracture surface features of a tensile fractured specimen (90^0 build angle orientation) with a GED of 1.67 J/mm² are shown in Figure 6. Unmelted powder particles and interlayer delamination due to incomplete fusion are clearly visible. Ductile fracture features are visible in the areas of complete fusion.

Tensile fracture morphology of 2.0 J/mm^2 energy density specimen

Stainless steel tensile specimen's fractured surface with a GED of 2.0 J/mm^2 (90^0 build angle orientation) is shown in Figure 7. A combination of ductile and brittle fracture features are visible in this fractograph. Fractured surface is characterized by the presence of a honey comb structure and relatively less ductile areas as indicated by relatively smoother/cleavage surfaces.
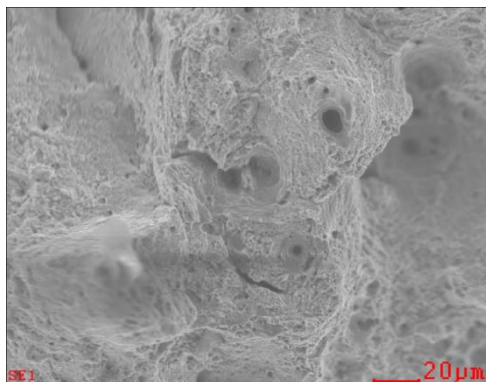

Fig. 7. Tensile fracture (energy density, 2.0 J/mm^2) surface showing honey comb structure and cleavage features at isolated locations

Tensile fracture morphology of 3.75 J/mm^2 energy density specimen

In Fig. 8 is presented the tensile fracture of the surface with unmelted particles and partial fusion.
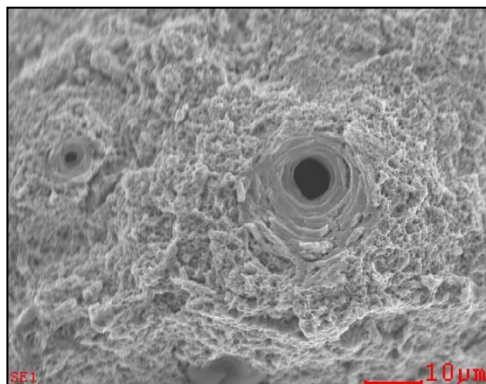

Fig. 8. Tensile fracture (energy density, 3.75 J/mm^2) surface revealing a highly ductile fracture features with voids

Figure 8 demonstrates the tensile fracture surface features of the specimen with a GED of 3.75 J/mm^3 (90^0 build angle orientation). Highly ductile failure, characterized by the presence of voids, fibrous features, is clearly visible.

Conclusions

The lowest energy density (1.67 J/mm^2) tensile specimens of 316L stainless steel demonstrated relatively more brittle fracture surface areas due to incomplete fusion of build layers during LPBF processing.

The highest energy density (3.75 J/mm^2) tensile specimens exhibited predominantly a ductile fracture as a result of complete melting and fusion of layers.

Mixed mode (ductile and brittle) fracture surface morphologies were observed for the 316L stainless steel tensile specimens produced with intermediate energy (2.0 J/mm^2) density.

Wrought fatigue fractured specimens showed dominant ductile fracture characteristics.

Fatigue fractured LPBF processed specimens demonstrated fibrous/ductile fracture for the specimens produced at 90^0 build angle.

Acknowledgement

References

[1] W. E. Frazier, *Metal Additive Manufacturing: A Review*, **Journal of Materials Engineering and Performance**, **3**, 2014, pp.1917-1928.

[2] D. D. Gu, W. Meiners, K. Wissenbach and R. Poprawe, *Laser additive manufacturing of metallic components: materials, process and mechanisms*, **International Materials Reviews**, **57**(3), 2012, pp. 133-164.

[3] S. Hamada, *Deformation and Damage Mechanisms in Ultrafine-Grained Austenitic Stainless Steel during Cyclic Straining*, **Metallurgical and Materials Transactions A**, **44**(4), 2013, pp. 1626-1630.

[4] M. L. Pace, A. Guarnaccio, P. Dolce, D. Mollica, G.P. Parisi, A. Lettino, L. Medici, V. Summa, R. Ciancio and A. Santagata, *3D additive manufactured 316L components microstructural features and changes induced by working life cycles*, **Applied Surface Science**, **418** (Part B), 2017, pp. 437-445.

[5] M. Zhang, Chen-Nan Sun, X. Zhang and H. Li, *Fatigue and fracture behavior of laser powder bed fusion stainless steel 316L: Influence of processing parameters*, **Materials Science and Engineering: A**, **703**(4), 2017, pp. 251-261.

[6] P.C. Collins, D.A. Brice, P. Samimi, I. Ghamarian and H.L. Fraser, *Microstructural control of additively manufactured metallic materials*, **Annual Review Materials Research**, **46,** 2016, pp. 63-91.

[7]   T. DebRoy, H.L. Wei, J.S. Zuback, T. Mukherjee, J.W. Elmer, J.O. Milewski, A.M. Beese, A. Wilson-Heid, A. De and W. Zhang, *Additive manufacturing of metallic components – Process, structure and properties*, **Progress in Materials Science**, **92**, 2018, pp. 112-224.

[8]   K. Guan, Z. Wang, M. Gao and X. Li, *Effects of processing parameters on tensile properties of selective laser melted 304 stainless steel*, **Materials & Design**, **50,** 2013, pp. 581–586.

[9]   P. Guo, B. C. Huang and H. Gao, *Study on microstructure, mechanical properties and machinability of efficiently additive manufactured AISI 316L stainless steel by high-power direct laser deposition*, **Journal of Materials Processing Technology**, **240,** 2017, pp. 12–22.

[10] J. D. Hunt, *Steady state columnar and equiaxed growth of dendrites and eutectic*, **Materials Science and Engineering**, **65,** 1984, pp. 75–83.

[11] J. J. Lewandowski and M. Seifi, *Metal additive manufacturing: a review of mechanical properties*, **Annual Review Materials Research**, **46,** 2016, pp. 151-186.

[12] C. Yan, L. Hao, A. Hussein, P. Young and D. Raymont, *Advanced lightweight 316L stainless steel cellular lattice structures fabricated via selective laser melting*, **Materials & Design**, **55**, 2014, pp. 533–541.

[13] E. Yasa and J. Kruth, *Microstructural investigation of selective laser melting 316L stainless steel parts exposed to laser re-melting*, **Procedia Engineering**, **19**, 2011, pp. 389–395.

[14] B. Zhang, L. Dembinski and C. Coddet, *The study of the laser parameters and environment variables effect on mechanical properties of high compact parts elaborated by selective laser melting 316L powder*, **Materials Science and Engineering A**, **584**, 2013, pp. 21–31.

[15] K. Zhang, S. Wang, W. Liu and X. Shang, *Characterization of stainless steel parts by laser metal deposition shaping*, **Materials & Design**, **55**, 2014, pp. 104–119.

[16] P. Rawn, *3D Printing of 316L Stainless Steel and its Effect on Microstructure and Mechanical Properties*, **https://digitalcommons.mtech.edu/grad_rsch/140**, 2017, pp. 1-88.

_____